



## Rapid interferometric imaging of printed drug laden multilayer structures

Sandler, Niklas; Kassamakov, Ivan; Ehlers, Henrik; Genina, Natalja; Ylitalo, Tuomo; Haeggstrom, Edward

*Published in:*  
Scientific Reports

*DOI:*  
[10.1038/srep04020](https://doi.org/10.1038/srep04020)

*Publication date:*  
2014

*Document version*  
Publisher's PDF, also known as Version of record

*Document license:*  
[CC BY-NC-ND](https://creativecommons.org/licenses/by-nc-nd/4.0/)

*Citation for published version (APA):*  
Sandler, N., Kassamakov, I., Ehlers, H., Genina, N., Ylitalo, T., & Haeggstrom, E. (2014). Rapid interferometric imaging of printed drug laden multilayer structures. *Scientific Reports*, *4*, 4020.  
<https://doi.org/10.1038/srep04020>



OPEN

# Rapid interferometric imaging of printed drug laden multilayer structures

SUBJECT AREAS:

INTERFERENCE  
MICROSCOPY

DRUG DELIVERY

Niklas Sandler<sup>1</sup>, Ivan Kassamakov<sup>2</sup>, Henrik Ehlers<sup>1</sup>, Natalja Genina<sup>1</sup>, Tuomo Ylitalo<sup>2</sup>  
& Edward Haeggstrom<sup>2</sup>Received  
8 August 2013Accepted  
14 January 2014Published  
7 February 2014Correspondence and  
requests for materials  
should be addressed to  
N.S. (niklas.sandler@  
abo.fi)

<sup>1</sup>Pharmaceutical Sciences Laboratory, Department of Biosciences, Abo Akademi University, Tykistökatu 6A, FI-20520 Turku, Finland, <sup>2</sup>Electronics Research Laboratory, Department of Physics, Division of Materials Physics, University of Helsinki, P.O. Box 64, FI-00014 Helsinki, Finland.

The developments in printing technologies allow fabrication of micron-size nano-layered delivery systems to personal specifications. In this study we fabricated layered polymer structures for drug-delivery into a microfluidic channel and aimed to interferometrically assure their topography and adherence to each other. We present a scanning white light interferometer (SWLI) method for quantitative assurance of the topography of the embedded structure. We determined rapidly in non-destructive manner the thickness and roughness of the structures and whether the printed layers containing polymers or/and active pharmaceutical ingredients (API) adhere to each other. This is crucial in order to have predetermined drug release profiles. We also demonstrate non-invasive measurement of a polymer structure in a microfluidic channel. It shown that traceable interferometric 3D microscopy is a viable technique for detailed structural quality assurance of layered drug-delivery systems. The approach can have impact and find use in a much broader setting within and outside life sciences.

Technology allows developing and fabricating pharmaceuticals in a tailored and personalized manner to meet the needs of individuals and patient groups<sup>1–3</sup>. The challenge is to deliver the benefits of this work to patients. Personalized medicine relies on diagnostic/genetic testing and targeted drug delivery. In addition our vision of future personalized medicine also entails flexible fabrication to allow accurate dosing of medicines. Personalized medicines can be e.g. produced by a scalable technology based on precise and robust 3D printing. Real-time quality control of the functionality of these drug delivery systems would be important and desirable.

A small, multi-layered, polymer structure can allow precisely controlled drug release in time and space with a carefully engineered release profile<sup>4,5</sup>. It can allow several active pharmaceutical ingredients to be released in temporal sequence. To assure the functionality of such a structure the thickness of the different layers should be tightly controlled, the layers need to adhere to each other, and the surface of the outermost layers must be intact<sup>6</sup>. The absolute measurement precision must be high because the layers are thin and because the drug release depends on layer thickness<sup>7</sup> and layer roughness<sup>8</sup>. The quality assurance method should be sterile and non-contacting to avoid contamination and altering the surface.

Our proposed contribution to personalized medicine is a method that combines 3D printing, 3D scanning white light interferometry (SWLI), and microfluidics to enable engineering and control of drug release profiles. Each of these three primary methods already alone provides impact. 3D printing gives reproducible otherwise unobtainable release profiles (it also permits high spot density, small volume spots and microarrays)<sup>9</sup>, SWLI provides non-contact, real time and non-invasive structural inference that can be metrologically traceable. Microfluidics can provide a clinically relevant and controllable, small volume environment where temperature and (bio)chemistry can be rapidly changed<sup>10</sup>.

In drug design and development one needs to control the properties of drug substances and additives in addition to enhancing and controlling their delivery and release<sup>3,6</sup>. Printing drugs allow fabricating structured and tailored drug-delivery systems. One can use topology (e.g. thickness and surface roughness of the printed layers) and chemical concentration to engineer their release profile<sup>6</sup>. These systems can be produced to tight specifications. Since material can be deposited accurately (space and amount) printed drugs with predetermined release profiles can potentially carry low drug concentrations. Quality assurance of printed products remains a challenge<sup>2,4</sup>.

2D and 3D printing permits fabricating functional structures of metals, polymers, and biomaterials<sup>11,12</sup>. 3D structures can be printed on a variety of surfaces with characteristic permeability, porosity, hydrophobicity/

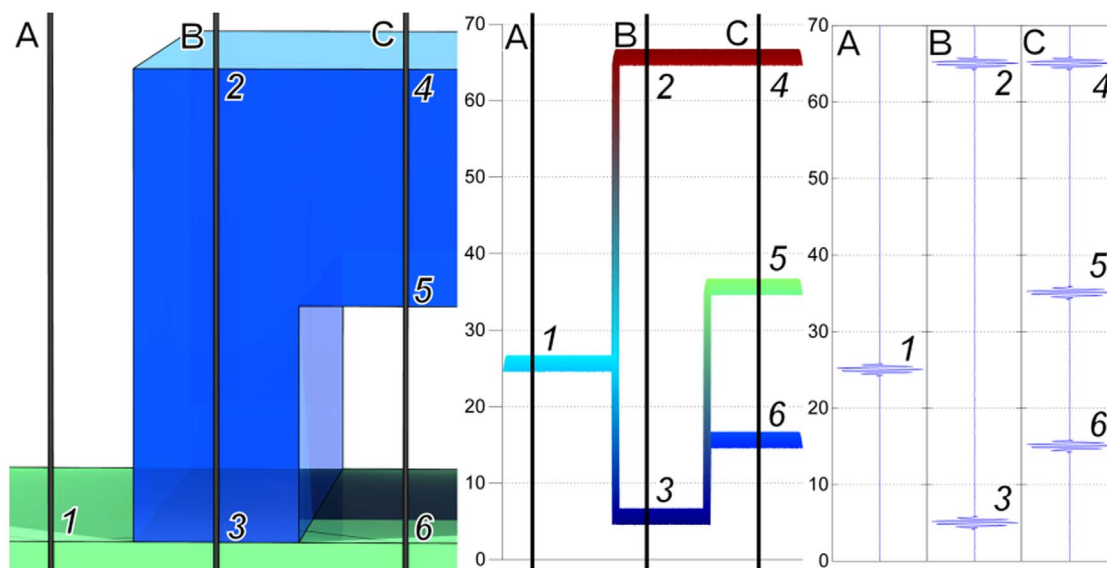


**Figure 1 | Scanning White Light Interferometer set-up that compensates for the microfluidic channel roof (Left).** The geometric thickness ( $d_g$ ) of the polymer layer is A1-B2 since the refractive index of air = 1. The effective refractive index of the adhered layer is (B3-B2)/(A1-B2). The same approach can be used to determine the height of disbands. The method provides 10–20 nm traceable resolution along the z-dimension. It can measure stacked layers that are static or moving<sup>10</sup>. It can determine a Sq parameter (ISO 25178) that potentially can be linked to Rq even inside a microfluidic channel without direct tactile access.

hydrophilicity and surface energy. This allows controlling the properties of the printed substances. Besides accurate patterning, printing on tailored functionalized substrates and multi-layer printing makes automated high-speed manufacture of complex structures possible. It opens up new avenues for tailoring physicochemical properties of organic substances.

There are few non-contacting and non-destructive ways to measure, in a traceable manner, surface roughness, thickness and adhesion of layers. Optical confocal microscopy provides sub-micron resolution along the z-direction (into the sample) but is disadvantageous for large area scanning. Moreover, it employs intense laser light, which may alter the mechanical and chemical properties of drug-laden polymers. Measuring inside a microfluidic channel is hard<sup>13</sup>. LED-based optical coherence tomography (OCT) even though a point-by-point method, fulfills many of the above requirements but its precision in determining the thickness of thin layers may be insufficient<sup>14</sup>. Ultra-sound microscopy especially used in second harmonic mode<sup>15</sup> provides qualitative images but seldom allows one to quantitatively determine the strength of adhesion or the size of disbands along the z-direction. Moreover it can't deal with gas-filled voids and usually requires acoustic couplants that may modify the sample. Terahertz imaging can infer about layered structures but does not provide sufficient quantitative spatial precision along the z-direction<sup>5</sup>. Nano-scale x-ray tomography potentially offers sufficient precision but is impractical since it is slow and uses ionizing radiation<sup>16</sup>. None of these methods fulfill the requirements presented by the current case (personalized drugs produced at point-of-care). Non-contacting, rapid, and non-destructive SWLI allow the possibility to determine surface roughness, the geometrical thickness of layered structures, the adherence between the layers, and the thickness of each individual layer<sup>17</sup>. Here we report the first implementation of scanning white light interferometry to study these features of layered drug-delivery systems.

## Results

Our custom-built SWLI optically compensates for the thickness of the roof in the microfluidic channel (Fig. 1) and measures the effective refractive index of the drug-laden structure (Fig. 2). The SWLI method provides 10–20 nm traceable resolution along the z-dimension. This

potentially sterile technique requires no sample preparation. Using image stitching it allows, when necessary, high resolution also across a large surface (up to 200×)<sup>18</sup>. Moreover, it can determine surface roughness Sq (ISO 25178) for an embedded surface without direct tactile access. It can measure stacked layers that are static or moving<sup>19</sup>.

SWLI measures the optical path difference between the reference and sample arm of the interferometer. When the sample is in air and we measure the step height - the single layer thickness - there are two interferences one for the base surface (Point A1, Fig. 1) and one for the top surface of the layer (Point B2, Fig. 1). The distance between these two interferences is equal to the layer thickness directly. When we measure through a well bonded layer there are also two interferences, but the position of the second one is shifted (Point B3, Fig. 1), compared to the interference at the base surface (Point A1, Fig. 1) because the optical thickness is equal to the geometrical thickness multiplied by the refractive index of the layer. The shift of the second interference depends of the refractive index of the layer (case B in the figure). The ratio between geometrical and optical thicknesses is equal to the refractive index of the layer. In the case of an unbonded or missing part of the layer a third interference appears between the first and second one (case C in the figure) and the shift of the last interferogram (Point C6, Fig. 1) depends of the thickness of the nonbonded layer.

To demonstrate the capacity of our proposed method a multi-layer drug-delivery system containing the vitamin B2, riboflavine sodium phosphate (RSP), is shown in Fig. 3a. Samples featuring these crossing lines of HPMC and RSP were placed on glass microscope cover slips. The image is 1 mm<sup>2</sup>. We prepared relevant test samples using a technique that simulated printing as described in<sup>5</sup>. The transparent HPMC lines were on average 3.98 μm thick and 5–10 mm wide whereas the RSP lines were on average 26 μm thick. The roughness of the HPMC (Sq1) was 0.58 μm and RSP (Sq2) 0.46 μm<sup>2</sup>. Figure 3a shows a disbonded HPMC-RSP multilayer system featuring air filled voids 0.15–30 μm tall. Figure 3b illustrates both adhered and disbonded multi-layer systems of hydroxypropylcellulose (HPC) film on a PET (polyethylene terephthalate) surface. These images show high resolution top surface topography with roughness of 0.31 μm (Sq1) and an apparently rougher second surface (light

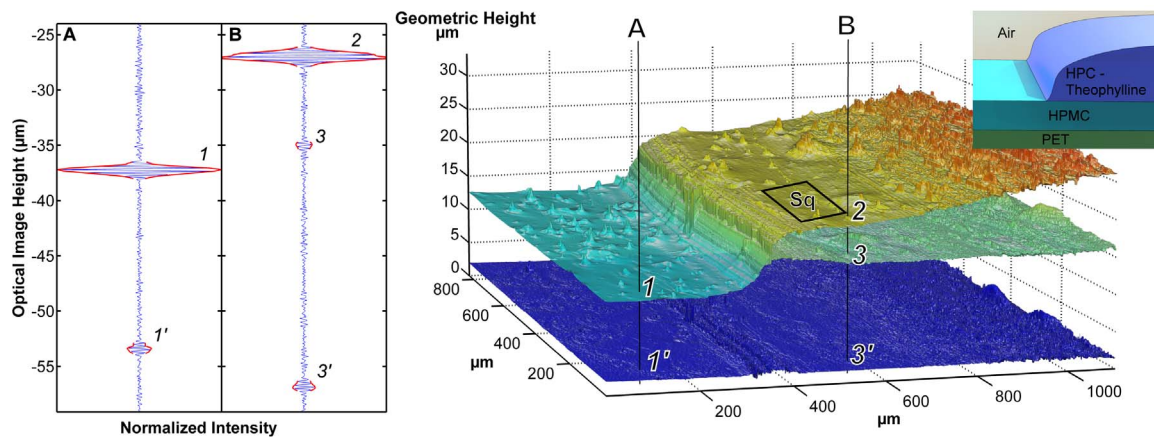


**Figure 2** | HPC-Theophylline laden layer on top of a HPMC layer residing on PET. Even without knowing the refractive index of the HPC-Theophylline layer the thickness can be determined (5  $\mu\text{m}$  on the left 10  $\mu\text{m}$  on the right). Sq on the indicated area is 0.157  $\mu\text{m}$ . **(Left)** Measured interferences. **(Inserts top right)** Schematic of the samples.

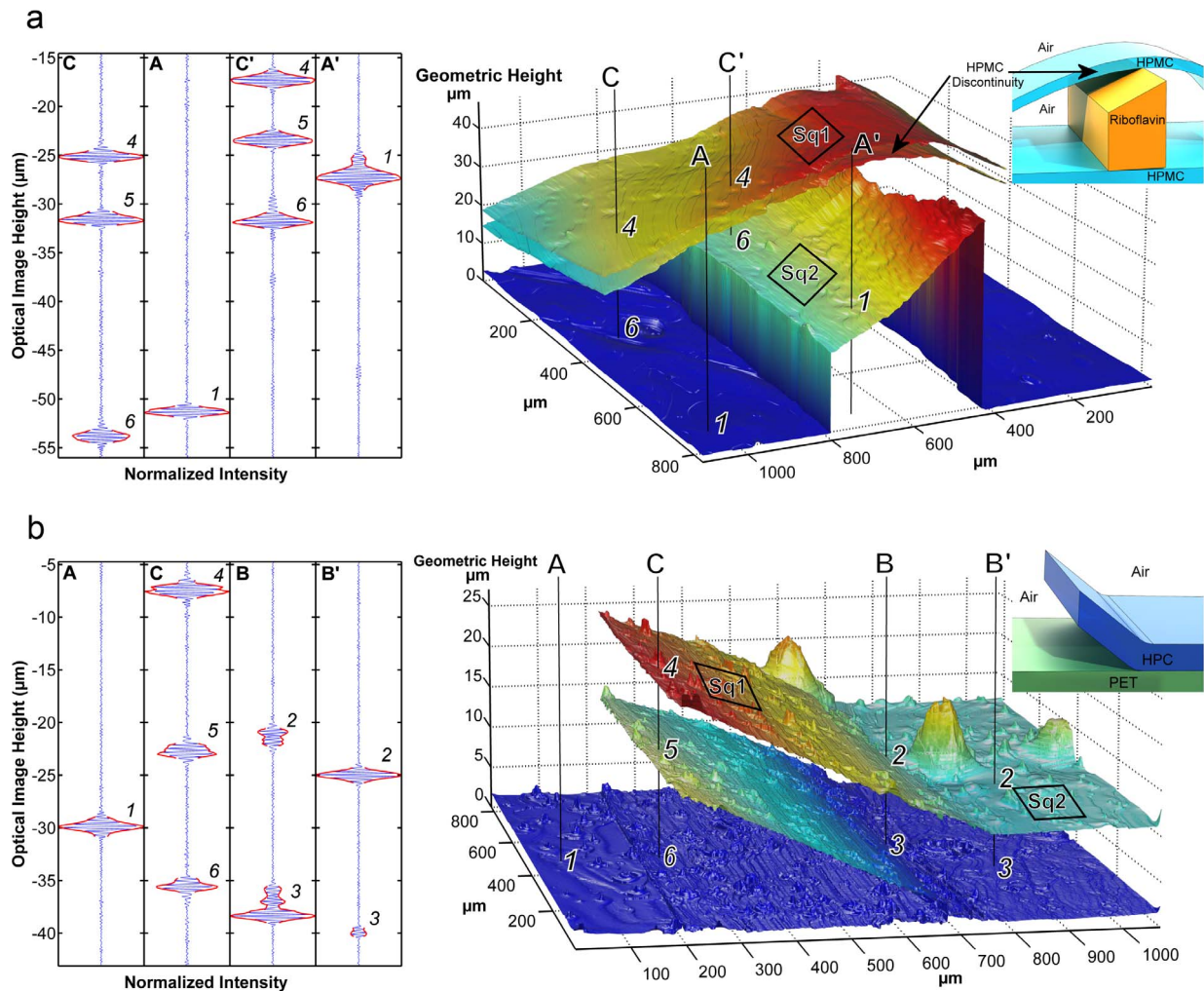


**Figure 3** | (a). Multilayer drug delivery system in the form of a crossing strip of printed riboflavin sodium phosphate (RSP) layer between two layers of hydroxypropyl methylcellulose (HPMC) film reconstructed from a SWLI measurement. (b). Structure of hydroxypropyl-cellulose (HPC) film on a PET surface revealing up to 13  $\mu\text{m}$  tall delamination, 0.31  $\mu\text{m}$  (Sq1) and 0.20  $\mu\text{m}$  (Sq2) surface roughness. **(Left)** Measured interferences, **(Inserts top right)** Schematic of the samples. We can determine surface topology with high resolution and we can determine presence of disbands in multilayer structures.

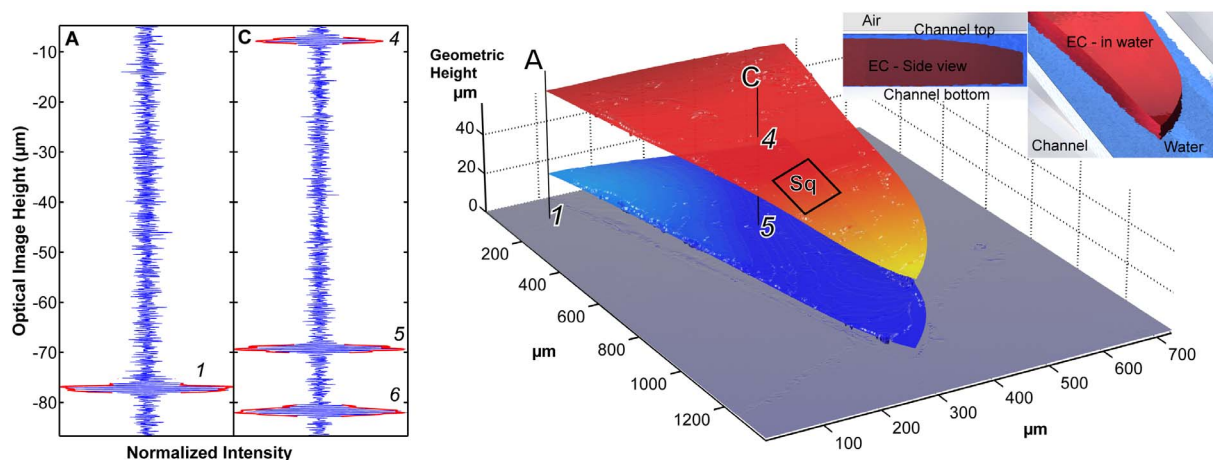


**Figure 4** | Left: (a) Interferograms and reconstructed SWLI image of printed ethylcellulose polymer film drug-delivery system imaged inside a microfluidic channel during 8  $\mu\text{l}/\text{min}$  water discharge. Indicated: DDS surfaces (top surface and bottom surface). The single camera pixel data - interferograms, were obtained for the corresponding points on the layers. Using the method outlined in Figure 1 we determined the refractive index ( $n = 1.47 \pm 0.02$ ), the average thickness (44.0  $\mu\text{m}$ ) of the structure, and the average height of the disbond (5.7  $\mu\text{m}$ ). The Sq in the indicated area is 0.30  $\mu\text{m}$ . Right: (b) The imaged structure.

dispersion by the top surface makes it appear rougher than it is). Single camera pixel data (Fig. 3a and 3b, leftmost) and a 3D surface plot of the polymer layer are shown (Fig. 3a and 3b, middle). The images were reconstructed pixel by pixel from the interferogram. The depth coordinate of each layer was extracted using Larkin's algorithm<sup>20</sup>. Fig. 2 shows how the geometric thickness of a structure can be determined even though its refractive index is not known in advance. The SWLI measures optical thickness  $d_{opt}$ . The geometric thickness ( $d_g$ ) of the polymer layer is  $A1-B3$  since the refractive index of air = 1. The effective refractive index of the adhered layer is  $(B3 - B4)/(A1 - B3)$ . The same approach can be used to determine both layer thickness and disbond height. Except for the top layer the depth coordinate was corrected using the refractive index. This index was obtained by relying on a discontinuity in the structure, see Fig. 3a. The interferograms from a point on the top layer and from a corresponding point on the bottom surface on that layer are separated on average by  $d_{opt} = 6.23 \mu\text{m}$  whereas the discontinuity on bottom surface is known to be 2.25  $\mu\text{m}$  tall which indicates an estimated layer thickness of 3.98  $\mu\text{m}$ . The height of the disbands was determined by assuming that the refractive index of the disbond was 1.00. Figure 4 shows a polymer structure measured inside a microfluidic channel during 8  $\mu\text{l}/\text{min}$  (1.8 mm/s) water flow. It took a few minutes to obtain the images in Fig. 3 and 4. These images were automatically analyzed by commercial and custom made software to construct and analyze 3D images of the cross-over point of the two crossing strips. The standard uncertainty for the z-coordinate in the construct was 0.045  $\mu\text{m}$ . We assumed the refractive index of water to be 1.33.

## Discussion

The proposed method rapidly determined the structure and presence of disbands in the printed drug-delivery system. There are limitations to the method. A layer separation, of less than 0.5  $\mu\text{m}$  or more than a few millimeters is hard to image. When the number of interfaces exceeds four it is hard to automatically extract the layers. The employed technique to derive the effective refractive index may not always work well. One example is high throughput analysis of systems with different drugs, another example is if the drug concentration exhibits a gradient inside a layer. Finally, the Sq value has not yet been linked in a traceable manner to a common surface roughness index such as Rq.

We presented for the first time a practical method for traceable structural quality assurance of printed drug delivery systems. This

result opens up a plethora of opportunities to induce quality assured fabrication in the field of tissue engineering, microfluidics, bio-MEMS, metamaterials, as well as nano- and micro-sized layered structures in addition to printed pharmaceuticals.

This traceable quantitative method can provide a competitive edge to both research and production carried out in academia and the industry. In practice one can carry out high throughput label-free testing, one can optimize products structurally, and one can assess systems in wet and dry environments. The method has high spatial and temporal precision, and can be applied in a controlled microfluidic environment. It can allow structural and functional quality assurance for a broad range of applications in life sciences.

## Methods

**Scanning white light interferometry (SWLI).** The samples were imaged using a custom-made SWLI instrument, Fig. 2. Briefly, the instrument uses a halogen lamp (Osram G4, driven at 6 Volts, 10 W), a standard 5 $\times$  Michelson Nikon objective (Nikon CF IC Epi Plan TI; Japan) or 10 $\times$  Mirau objective (Nikon CF IC Epi Plan DI; Japan), and a piezo translator with 100  $\mu\text{m}$  travel (Physik Instrumente - type P-721.CDQ). The system magnification was 3.15 with the Michelson objective and 6.3 with the Mirau objective. The instrument can determine profiles with  $\pm 15 \text{ nm}$  accuracy along the z-direction. A detailed description of the VIS interferometer is given in<sup>17</sup>. In the receiving part we employed a 3.63  $\mu\text{m}$  pixel size black and white camera (Hamamatsu C11440 Orca Flash2.8, Hamamatsu City, Japan).

We validated the SWLI for top surface imaging by inspecting a standard sample VLSI 1853  $\pm 2.3 \text{ \AA}$  (model #SHS-1800 QC, VLSI Standards, Inc.). Traceability to the national SI standard is ensured using a transfer artifact. The influence of the roof of the channel was removed with a compensating plate identical to the 200  $\mu\text{m}$  thick cover glass (CLS2960246, Sigma-Aldrich, Corning) of the microfluidic channel inserted into the reference arm of the interferometer.

**Microfluidic channels.** The cover glass and 1000  $\mu\text{m}$  thick microscope base glass were used (Menzel Microscope slides, ISO 8037/1) to construct the microfluidic channels. Inlet and outlet holes (2 mm in diameter) were drilled in the base glass. Plastic tubing (TubPEEK Blu 1/16 Z226661) was attached by UV cured glue (Thorlabs NOA81). The tubes were leveled to the base glass. A 2 mm wide channel was created using two-sided 50  $\mu\text{m}$  thick double-sided tape (Tesa) between the cover and base glass. The sample was placed in the middle of the channel. The cover glass was then attached. Ion-exchanged water was flowed through the channel with a pump (Alladdin-1000, World precision Instruments, Aston, Stevenage, UK).

**Sample preparation.** There were four kinds of samples. The films were created by solvent casting using a manual pipette (BioHit ProLine + Mech, Finland) simulating printing of drug substances and polymers as described in<sup>2</sup>. All samples were dried in ambient conditions (21 $^\circ\text{C}$  and 40% RH). The aqueous solutions for Figure 3 membranes consisted either of 2 mg/ml riboflavin sodium phosphate (RSP, riboflavin 5'-monophosphate sodium salt, Ph. Eur., Fluka Analytical, Sigma-Aldrich, France) in 1% (w/w) hydroxypropyl methylcellulose (HPMC, Metolose 90SH-4000, Shin-Etsu, Tokyo, Japan) or pure 1% HPMC solution. The sample presented in



Figure 3a was a three-layer construct (HPMC/RSP-HPMC/HPMC, from top to bottom) prepared on a water impermeable polyethylene terephthalate (PET) film (Mylar® A, Dupont Teijin Films Europe, Luxembourg). The sample in Figure 3b was a two-layer construct with hydroxypropylcellulose (HPC, Klucel LF, Shin-Etsu, Tokyo, Japan) residing on a PET surface (HPC/PET, from top to bottom). The HPC film was prepared by deposition of 1% HPC solution on top of the PET surface. The solution to fabricate the film for the sample in Fig. 4 contained water insoluble ethylcellulose (EC, E8003, Sigma-Aldrich, USA; ethoxy content, 48–49.5%; viscosity, 45 cP) and ethanol ( $\geq 96.1\%$ , Etax A, Altia OYj, Finland). The EC sample was placed in a microfluidic channel for measurement. Fig. 2 depicts a three-layer construct (theophylline-HPC/HPMC/PET, from top to bottom). The solutions to create these double-layer membranes contained 7 mg/ml theophylline in 3.3% (w/w) hydroxypropylcellulose (HPC, in ethanol) (top layer) and 1% HPMC (in water) (second layer). These two layers were made on top of a PET surface. Incisions through the double-layer membrane were made to remove a section of the system to allow determining the film thickness and its attachment to the PET-base in Fig. 2.

**Image reconstruction and processing.** We scanned the samples with our custom-made SWLI instrument. Images were acquired with 68.75 nm vertical spacing. At each height we averaged 10 camera frames after which we recorded both the average image and the height coordinate output by the calibrated piezo capacitive sensor.

Surfaces were reconstructed using Larkin's algorithm<sup>7</sup> on a high-pass filtered SWLI signal. This modification permitted us to do multi-surface feature extraction. Shortly: the single pixel camera intensity data vector (stacked pixels) was high-pass filtered with a second order derivative filter. The algorithm then identified and stored the maximum of the envelope of the interferences in the filtered vector. The interactive multi-interface extraction process first asked for the maximum number of interfaces to extract, and for the minimum permissible threshold value for envelope maxima and interface separation. For each 3D image the threshold value was found by an iterative procedure. (In Fig. 2 the HPC Theophyllin - HPMC interface was found by pooling 25 pixels prior to extracting envelope maxima. Extracted interfaces were filtered using first a  $3 \times 3$  pixel filter and then a  $7 \times 7$  pixel median filter along the x-y direction. Surface height data was corrected from optical height to geometric height using the method illustrated in Fig. 2. In practice, planes were fitted in least squares sense to the reference surfaces #1 and #3 in the above figure. The distance between these planes was determined analytically. Local surface fitting (second or third order in x and y) was used to patch small areas lacking data. These areas were identified and the size of the patch was decided manually *post hoc*. The final 3D image was tilt-corrected by requiring that the bottom most interface was horizontal. The Sq parameter was determined from unfiltered surface data as outlined in ISO25178.

- de Gans, B.-J., Duinevald, P. C. & Schubert, U. S. Inkjet printing of polymers: state of the art and future developments. *Adv. Mat.* **16**, 203–213 (2004).
- Sandler, N. *et al.* Inkjet printing of drug substances and use of porous substrates – towards individualized dosing. *J. Pharm. Sci.* **100**, 3386–3395 (2011).
- Datta, S. & Grant, D. J. W. Crystal structures of drugs: advances in determination, prediction and engineering. *Nature Rev. Drug Discovery* **3**, 42–57 (2004).
- Genina, N. *et al.* Tailoring controlled-release oral dosage forms by combining inkjet and flexographic printing techniques. *Eur. J. Pharm. Sci.* **47**, 615–622 (2012).
- Hamburg, M. A. & Collins, F. S. The Path to personalized medicine. *N. Engl. J. Med.* **363**, 301–304 (2010).
- Qiu, Y. *Developing Solid Oral Dosage Forms* (Elsevier Inc., New York, the United States 2009).

- Ho, L. *et al.* Applications of terahertz pulsed imaging to sustained-release tablet film coating quality assessment and dissolution performance. *J. Controlled Release* **119**, 253–261 (2007).
- Karagkiozaki *et al.* Development of a nanoporous and multilayer drug-delivery platform for medical implants. *Int. J. Nanomedicine*. **7**, 5327–5338 (2012).
- Lee, B. K. *et al.* Fabrication of drug-loaded polymer microparticles with arbitrary geometries using a piezoelectric inkjet printing system. *Int. J. Pharm.* **427**, 305–310 (2012).
- Huh, D. *et al.* A Human Disease Model of Drug Toxicity-Induced Pulmonary Edema in a Lung-on-a-Chip Microdevice. *Sci. Transl. Med.* **4**, 147–159 (2012).
- Setti, L. *et al.* An amperometric glucose biosensor prototype fabricated by thermal inkjet printing. *Biosens. Bioelectron.* **20**, 2019–2026 (2007).
- Calvert, P. Inkjet Printing for Materials and Devices. *Nature* **428**, 911–918 (2004).
- Bornhop, D. J. *et al.* Free-Solution, Label-Free Molecular Interactions Studied by Back-Scattering Interferometry. *Science*. **317**, 1732–1736 (2007).
- Petzold, A. *et al.* Optical coherence tomography in multiple sclerosis: a systematic review and meta-analysis. *The Lancet Neurology*. **9**, 921–932 (2010).
- Mogensen, M. *et al.* In vivo thickness measurement of basal cell carcinoma and actinic keratosis with optical coherence tomography and 20-MHz ultrasound. *Brit. J. Dermatology* **160**, 1026–1033 (2009).
- Dierolf, M. *et al.* Ptychographic X-ray computed tomography at the nanoscale. *Nature* **467**, 436–439 (2010).
- de Groot, P., Colonna de Lega, X. & Liesener, J. Model-based white light interference microscopy for metrology of transparent film stacks and optically-unresolved structures Fringe 2009 (Springer, USA, 2009).
- Hanhijärvi, K. *et al.* Scratch resistance of plasticized hydroxypropyl methylcellulose (HPMC) films intended for tablet coatings. *Eur. J. Pharm. Biopharm.* **74**, 371–376 (2010).
- Kassamakov, I. *et al.* Scanning white light interferometry with a supercontinuum source. *Opt. Lett.* **34**, 1582–1584 (2009).
- Larkin, K. G. Efficient nonlinear algorithm for envelope detection in white light interferometry. *JOSA A*. **13**, 832–843 (1996).

## Acknowledgments

We acknowledge Mr. Ville Heikkinen for building the microfluidic channels and Mr. Ossi Saresoja for implementing the interface extraction algorithm.

## Author contributions

N.S., I.K. and E.H. Conceived the experiments. N.G. prepared the samples, H.E., N.G. and T.Y. carried out the experiment, N.S., I.K., H.E. and E.H. analyzed the data, all authors discussed the results and contributed to the manuscript.

## Additional information

**Competing financial interests:** The authors declare no competing financial interests.

**How to cite this article:** Sandler, N. *et al.* Rapid interferometric imaging of printed drug laden multilayer structures. *Sci. Rep.* **4**, 4020; DOI:10.1038/srep04020 (2014).



This work is licensed under a Creative Commons Attribution-NonCommercial-NoDerivs 3.0 Unported license. To view a copy of this license, visit <http://creativecommons.org/licenses/by-nc-nd/3.0>